A comparison study of mixed convection heat transfer of turbulent nanofluid flow in a three-dimensional lid-driven enclosure with a clockwise versus an anticlockwise rotating cylinder

Ali Khaleel Kareem [a, b,*], Shian Gao [a]

[a] Department of Engineering, University of Leicester, Leicester LE1 7RH, United Kingdom
[b] Engineering Department, University of Thi-Qar, 64001 Nassiriya, Iraq

Abstract

A turbulent 3D mixed convective flow of pure water, H_2O, and nanofluid, SiO_2-H_2O, inside a differentially heated moving wall enclosure containing an insulated rotating cylinder over a range of rotational speeds, $-5 \leq \Omega \leq 5$, Reynolds numbers, 5000 and 10000, and constant Grashof number, is numerically investigated. A cooled lid-driven top wall and a heated bottom wall are the only thermally uninsulated walls in this domain. A standard k-ε for the Unsteady Reynolds-Averaged Navier-Stokes (URANS) approach is applied to the turbulence calculation. Nusselt number, mean velocity profile, streamline, isothermal and isosurface temperatures are derived and presented in this paper to gain a better understanding of the effects of clockwise and anti-clockwise rotating cylinder directions on the heat transfer and flow patterns. Interesting changes in flow structure and heat transfer have been analysed for all rotational speeds and fluid types at both Reynolds number values. Nonlinear increases in Nusselt number have been observed by using nanofluid instead of pure water. The wall shear stress and turbulent kinetic energy profiles are found to be influenced by changing the Reynolds number and rotational speed and direction. Furthermore, incremental heat transfer rates at the walls can be achieved by increasing the cylinder rotation speeds, but these increases have weaker influences on the top wall than on the bottom wall.

Keywords: *Mixed convection, Rotating cylinder, Lid-driven cavity, Turbulent flow, URANS.*

**Corresponding author at: Department of Engineering, University of Leicester, Leicester LE1 7RH, United Kingdom. Tel: +44 (0)116 252 2874; fax: +44 (0)116 2522525.*

Email address: akkak2@le.ac.uk, alikhaleel17@yahoo.com (A.K. Kareem).

1. Introduction

The mixed convective flow of moving wall cavity is produced as a result of both natural and forced convection. Since heat convection can be represented in many cavity configurations it has many industrial and engineering applications such as electronic cooling, lubrication technologies, oil extraction, solar collectors, food processing [1-8], many researchers have investigated various free or mixed convection problems. Involving some additional passive objects within the enclosure to enhance the heat transfer ratio has become popular over the years. Sun, et al. [9] added a triangular fin to control the heat transfer of the mixed convection case.

Nomenclature

CFL	Courant–Friedrichs–Lewy number	Y	distance along the non-dimensional y-coordinate (y/H)
D	width of the cavity on z-axis (m)	Z	distance along the non-dimensional z-coordinate (z/D)
d	cylinder diameter (m)		
FVM	finite volume method		
Gr	Grashof number ($g\beta_m\Delta TW^3/v_m^2$)	*Greek symbols*	
h	convective heat transfer coefficient (W/m^2K)	α	thermal diffusivity of the fluid (m^2/s)
k	turbulent kinetic energy (m^2/s^2)	β	volumetric coefficient of thermal expansion (1/K)
L	width of the cavity on x-axis (m)	μ	dynamic viscosity of the fluid (Pa/s)
Nu	Nusselt number	v	kinematic viscosity of the fluid (m^2/s)
Pr	Prandtl number (v_m/α_m)	ρ	density of the fluid (kg/m^3)
Re	Reynolds number ($U_{0,m}W/v_m$)	ε	dissipation rate of turbulent kinetic energy (m^2/s^3)
Ri	Richardson number (Gr/Re^2)	ω	rotational speed (rad/s)
$\bar{S}_{ij}$	large-scale strain rate tensor for grid-filter	Ω	dimensionless rotational speed
T	temperature of the fluid (K)	*Subscripts*	
t	time	av	average value
u	velocity component at x-direction (m/s)	b	buoyancy
U	dimensionless velocity component at x-direction	C	value of cold temperature
U_0	lid velocity (m/s)	H	value of hot temperature
v	velocity component at y-direction (m/s)	rms	root mean square
V	dimensionless velocity component at y-direction	sgs	sub-grid scale
W	dimensionless velocity component at z-direction	t	turbulent
x	distance along the x-coordinate		
X	distance along the non-dimensional x-coordinate (x/L)		

Inserting a circular body to enhance the heat transfer of a lid-driven cavity was investigated by Oztop, et al. [10]. Appending a heated triangular block at the centre the top moving wall square enclosure has an impact on the heat transfer coefficient [11]. Studying the effects of

both inserting an isothermal square object and using a nanofluid inside a lid-driven square enclosure on the heat transfer ratio was undertaken by Mehmood, et al. [12].Nonetheless, it may be noticed that neither the 3D domain nor turbulent flow condition has been used in the above references.

Moreover, some studies of mixed convection have been completed by introducing one cylinder or more within the enclosures to control and increase the heat transfer ratio. A 2D laminar mixed convection heat transfer of nanofluid within a moving wall square enclosure containing a rotating cylinder was considered by Mirzakhanlari, et al. [13] to study the impacts of the Richardson number and rotational speed. It was demonstrated that increasing either the Richardson number or the nanofluid speed causes an enhancement in heat transfer ratio, while increasing the rotational speed of the cylinder has a negative effect on the heat transfer ratio. A 2D free convection study of a laminar power-law fluid within a square cavity containing a heated cylinder was completed by Shyam, et al. [14], which concentrated on the effects of changing the cylinder location along the vertical central line for different dimensionless parameters. It was realised that the heat transfer ratio and streamline and isotherm contours can be affected by changing the Grashof and Prandtl number or cylinder location. A study of 2D laminar natural convection of air within a cold-walled square enclosure containing a stationary sinusoidal cylinder was undertaken by Nabavizadeh, et al. [15] to evaluate the influences of different angles, amplitudes and number of cylinder undulations. It was observed that changing cylinder parameters can affect the heat transfer and fluid patterns. Three-dimensional free convection of laminar flow within an enclosure containing a cylinder was simulated by Souayeh, et al. [16] in order to understand the impact of inclination angles of the cylinder at different Rayleigh numbers on the fluid patterns and heat transfer ratio. It was noted briefly that a significant effect was discovered regarding the heat transfer ratio, especially when the Rayleigh number is 10^6 and inclination angle is 90°. Limited research has been completed into mixed convection turbulent flow within lid-driven enclosures by utilizing an unsteady approach such as URANS (Unsteady Reynolds-Averaged Navier-Stokes) and LES (Large Eddy Simulation). Combined convection heat and mass transfer of water within a lid-driven cavity was studied by Kareem, et al. [1] to analyse the 3D flow structure and heat transfer by involving unsteady RANS and LES methods at various Reynolds numbers. The results have shown the ability of both methods to deal with the vortices of the turbulent flow. Nevertheless, secondary eddies were dealt with more comprehensively by utilizing the LES method. In addition, it was concluded that a remarkable effect on the heat transfer ratio and fluid patterns can be observed when the Reynolds number increases. Two different turbulent methods are used by Kareem and Gao [17] to study a combined mixed convection of different nanofluid types within a 3D moving sidewalls enclosure. It was demonstrated that heat transfer

and flow pattern can be influenced by adding nanoparticles to the pure fluid, and that the influence of the ratio could be changed by using different types, diameters and concentrations of nanoparticles. A clear difference in heat transfer rate has also been noticed by utilizing different turbulence methods.

Studies into various nanofluid types within cavities have been described by a number of researchers because of its considerable effect on heat transfer enhancement. Investigation of free and combined convective heat transfer of a differentially heated circular cylinders within an adiabatic cavity containing nanofluid was studied by Garoosi and Hoseininejad [18]. The influences of nanofluid thermophysical properties and the number of cold cylinders that the cavity contained and their location and rotational directions are considered at different Rayleigh and Richardson numbers. It has been found that increasing or decreasing heat transfer rate strongly depends on these parameters. Kareem, et al. [19] studied a laminar mixed convection of heat and mass transfer in a 2D trapezoidal moving wall enclosure that is filled with different types of nanofluid in a numerical manner. The authors aimed at an understanding of the effects of nanofluid type, nanoparticle diameter, inclined sidewall angle, aspect ratio, flow direction and Richardson number on the heat transfer ratio and flow distribution. It was concluded that SiO_2-H_2O showed the highest Nusselt number and aiding flow direction provides for a higher heat transfer ratio. In addition, it has been found that increasing the nanoparticle concentration and aspect ratio leads to an increase in the heat transfer coefficient, unlike when the nanoparticle diameter and inclination angle are increased.

It can be summarized from the current literature review that a study considering the effects of three-dimensional rotating cylinders in terms of their speeds and directions (clockwise and anticlockwise) within a top lid-driven closed cavity on turbulent nanofluid flow, and involving the unsteady RANS method, is unprecedented, and this consequently forms the main objectives of this paper.

2. Numerical model

2.1. Physical model

A sketch of the three-dimensional flow within a lid-driven cavity configuration containing a rotating cylinder is shown in Fig. 1. This study deals with an adiabatic central cylinder of diameter, d = 0.2 L, that rotates in the anticlockwise and clockwise directions within the lid-driven cavity with a heated bottom wall and moving cooled wall. The other remaining cavity walls are assumed to be adiabatic and stationary.

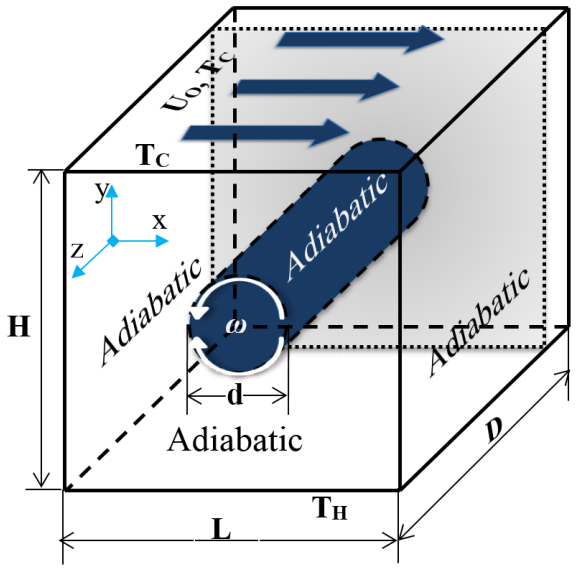

Fig. 1. Schematic of the analysed configuration.

2.2. Governing equations

An incompressible Newtonian fluid of unsteady flow has been used in this paper. The three-dimensional equations governing the continuity, momentum and energy are presented as follows [1, 20, 21]:

Continuity equation:

$$\frac{\partial u_i}{\partial x_i} = 0 \tag{1}$$

Momentum equation:

$$\frac{\partial u_i}{\partial t} + \frac{\partial (u_j u_i)}{\partial x_j} = -\frac{\partial P}{\partial x_i} + \frac{1}{Re}\left(\frac{\partial^2 u_i}{\partial x_i \partial x_i}\right) + \frac{Gr}{Re^2}\theta \tag{2}$$

Energy equation:

$$\frac{\partial (\theta)}{\partial t} + \frac{\partial (u_j \theta)}{\partial x_i} = \frac{1}{RePr}\left(\frac{\partial^2 \theta}{\partial x_i \partial x_i}\right) \tag{3}$$

Equations (4) and (5) below represent the turbulent kinetic energy (k) and the dissipation rate (ε) [22], Respectively.

The standard k-ε turbulence model is given by:

$$\frac{\partial}{\partial t}(\rho k)+\frac{\partial}{\partial x_i}(\rho k u_i)=\frac{\partial}{\partial x_j}\left[\left(\mu+\frac{\mu_t}{\sigma_k}\right)\frac{\partial k}{\partial x_j}\right]+P_k+P_b-\rho\varepsilon+S_k \quad (4)$$

$$\frac{\partial}{\partial t}(\rho \varepsilon)+\frac{\partial}{\partial x_i}(\rho \varepsilon u_i)=\frac{\partial}{\partial x_j}\left[\left(\mu+\frac{\mu_t}{\sigma_\varepsilon}\right)\frac{\partial k}{\partial x_j}\right]+C_{1\varepsilon}\frac{\epsilon}{k}(P_k+C_{3\varepsilon}P_b)-C_{2\varepsilon}\rho\frac{\epsilon^2}{k}+S_\varepsilon \quad (5)$$

where $C_{1\varepsilon}$, $C_{2\varepsilon}$ and $C_{3\varepsilon}$ are model constants and S_k and S_ε refer to the user-defined source terms. The remaining terms are written in equations (6-8).

Turbulent viscosity: $$\mu_t=\rho C_\mu\frac{k^2}{\varepsilon} \quad (6)$$

Production of k: $$P_k=-\rho\overline{u_i'u_j'}\frac{\partial u_j}{\partial x_i} \quad (7)$$

Effect of buoyancy: $$P_b=\beta g_i\frac{\mu_t}{Pr_t}\frac{\partial T}{\partial x_i} \quad (8)$$

2.3. Boundary conditions

The boundary conditions for the current study are defined as:

Top wall:

$\theta=0, U=U_{lid}, V=0, W=0$

Bottom wall:

$\theta=1, U=0, V=0, W=0$

Other walls:

$\partial\theta/\partial Y=0, U=0, V=0, W=0$

Adiabatic cylinder:

$\omega=\frac{\Omega\times 2U_0}{d}, d=0.2L$

2.4. Thermophysical properties of working fluids

Table 1 shows the thermophysical properties of pure water and SiO_2 nanoparticles. This paper uses a SiO_2 nanoparticle diameter of 25 nm and a volume fraction of 5%. The effective thermophysical properties of the nanofluid formed are calculated by utilizing equations (9-17).

135 Table 1

136 Thermophysical properties of pure water and SiO_2.

	ρ (kg/m³)	C_p (J/kg. K)	k (W/m. K)	μ (Ns/m²)	$\beta \times 10^{-5}$(K^{-1})
Pure Water (H_2O)	996.5	4181	0.613	0.0001	21
Silicon Dioxide (SiO_2)	3970	765	36	–	0.63

137

The effective thermal conductivity can be obtained by using the following mean empirical correlations [23]:

$$k_{eff} = k_{Static} + k_{Brownian} \quad (9)$$

$$k_{Static} = k_f \left[\frac{(k_{np} + 2k_f) - 2\phi(k_f - k_{np})}{(k_{np} + 2k_f) + \phi(k_f - k_{np})} \right] \quad (10)$$

$$k_{Brownian} = 5 \times 10^4 \beta \, \phi \rho_f C_{p,f} \sqrt{\frac{kT}{2\rho_{np} R_{np}}} \mathrm{f}(\mathrm{T}, \phi) \quad (11)$$

The effective viscosity can be obtained using the following mean empirical correlations [23]:

$$\mu_{eff} = \mu_{Static} + \mu_{Brownian} \quad (12)$$

$$\mu_{Static} = \mu_f / (1 - \phi)^{2.5} \quad (13)$$

$$\mu_{Brownian} = 5 \times 10^4 \beta \, \phi \, \rho_f \sqrt{\frac{k\,T}{2\rho_{np} R_{np}}} \mathrm{f}(\mathrm{T}, \phi) \quad (14)$$

where:

Boltzmann constant, *k*: $k = 1.3807 \times 10^{-23}$ *J/K*

Modelling function, *β*: $\beta = 0.0137(100\,\phi)^{-0.8229}$ for $\phi < 1\%$

$\beta = 0.0011(100\,\phi)^{-0.7272}$ for $\phi > 1\%$

Modelling function, $\mathrm{f}(\mathrm{T}, \phi)$:

$$\mathrm{f}(\mathrm{T}, \phi) = (-6.04\phi + 0.4075)T + (1722.3\phi)$$

The nanofluid density ρ_{nf} can be obtained from the following equation [23]:

$$\rho_{nf} = (1 - \phi)\rho_f + \phi\rho_{np} \quad (15)$$

where ρ_f and ρ_{np} are the mass densities of the base fluid and the solid nanoparticles, respectively.

The effective heat capacity at constant pressure of the nanofluid $(C_p)_{nf}$ can be calculated from the following equation [23]:

$$(\rho C_p)_{nf} = (1 - \phi)(\rho C_p)_f + \phi(\rho C_p)_{np} \quad (16)$$

where, $(C_p)_f$ and $(C_p)_{np}$ are the heat capacities of the base fluid and nanoparticles, respectively.

The effective coefficient of thermal expansion for the nanofluid $(\beta)_{nf}$ can be obtained from the following equation [24]:

$$(\rho\beta)_{nf} = (1 - \phi)(\rho\beta)_f + \phi(\rho\beta)_{np} \quad (17)$$

where $(\beta)_f$ and $(\beta)_{np}$ are thermal expansion coefficients of the base fluid and the nanoparticles, respectively.

138

139 *2.5. Numerical procedure*

140 Two different fluids have been used as working fluids inside the enclosure in order to compare
141 the nanofluid with a conventional fluid. The present study has used the finite volume method
142 and SIMPLIC algorithm to solve the governing equations of heat and mass transfer, and the
143 pressure-velocity coupling equations by utilizing the commercial CFD code ANSYS©FLUENT
144 (version R16.2) [25]. The convection and time evolution terms were dealt with using QUICK
145 and an implicit second-order scheme. The standard k-ε turbulence model was used for the
146 unsteady Reynolds-Averaged Navier-Stokes equations. The convergence criterion was
147 chosen as 10^{-5}.

148 *2.6. Code validation*

149 The present CFD models have been validated against a number of reports in the literature in
150 order to obtain a trusted numerical solver for the new simulations reported in this paper. The
151 first comparison was completed for the problem of the 2D steady mixed convection heat
152 transfer of a lid-driven enclosure containing a clockwise rotating cylinder as originally reported
153 by Chatterjee, et al. [26]. It can be observed from Fig. 2 and Fig. 3 that the comparisons of the
154 dimensionless velocity profiles along the vertical line at x = 0.25 and the isotherms and
155 streamlines show a good agreement. Fig. 4 demonstrates that the second comparison was
156 achieved successfully against the results originally reported by Alinia, et al. [27] for the
157 problem of the 2D laminar mixed convection heat transfer of a nanofluid within an inclined
158 moving wall cavity.

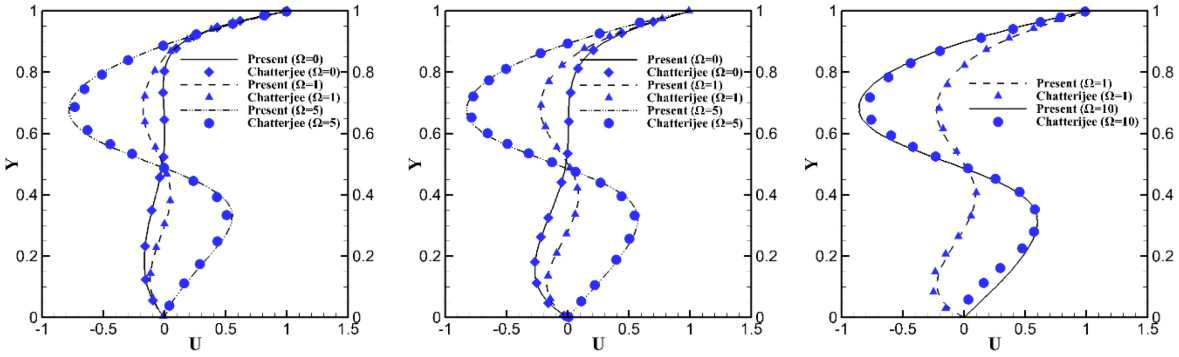

(a) Ri = 1 (b) Ri = 5 (c) Ri = 10

Fig. 2. Comparison of the present work of the dimensionless velocity profiles along the vertical line at x = 0.25 with that of Chatterjee, et al. [26].

159

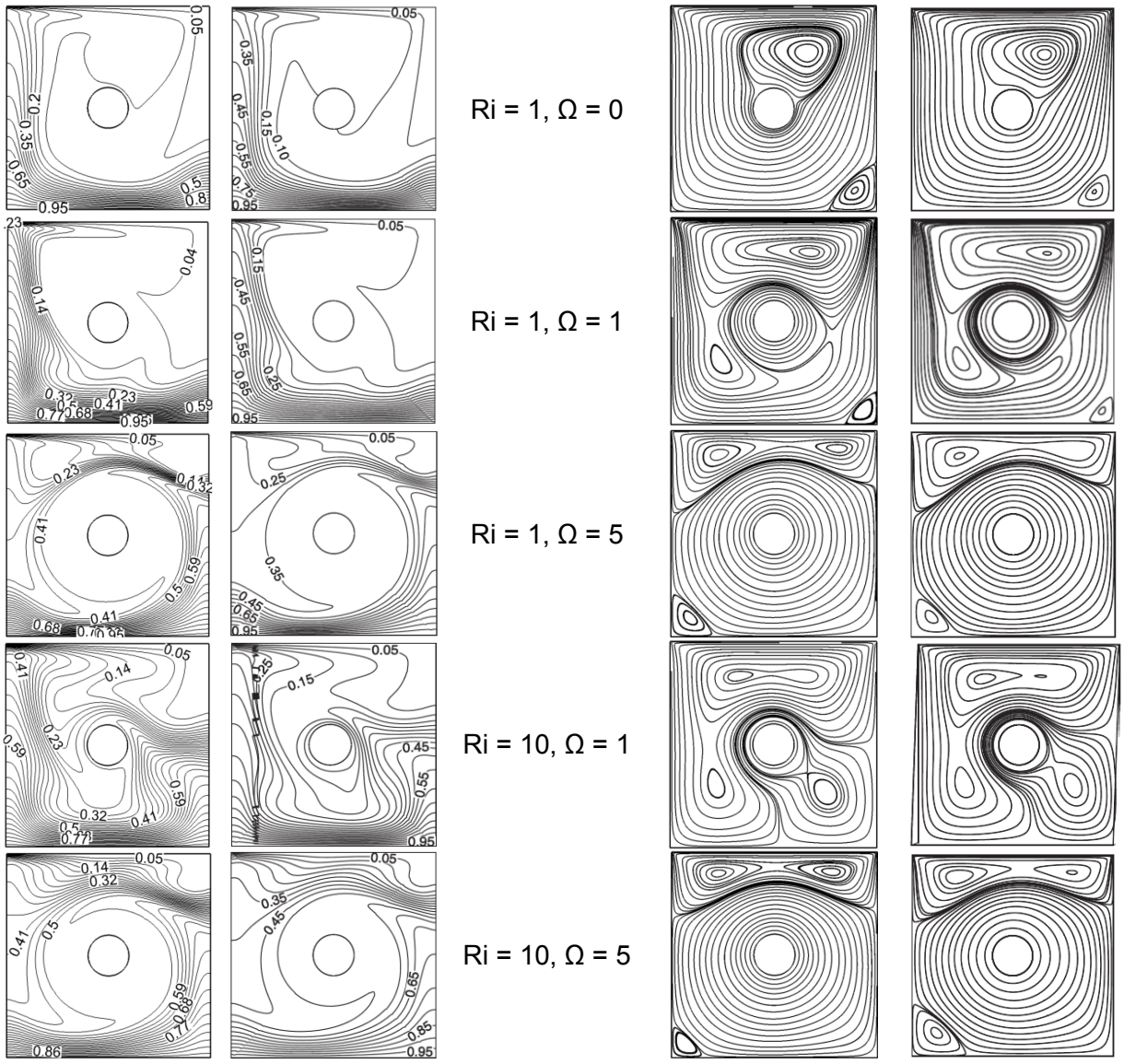

Fig. 3. Comparison of the present work of the isotherms and streamlines with Chatterjee, et al. [26].

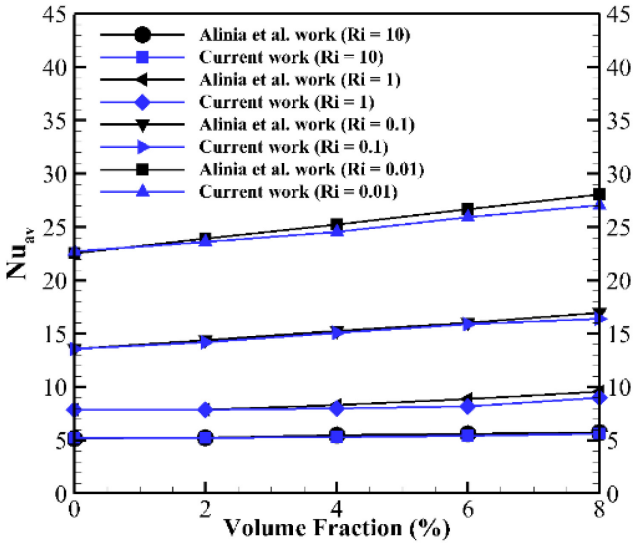

Fig. 4. Comparison of the current results of different nanoparticle concentrations and different Richardson numbers with Alinia, et al. [27].

2.7. Grid independence test

Structured and non-uniform grids that were considerably finer in the vicinity of the cavity walls and around the cylinder are used to discretise the domain. Five different numbers of mesh (125868, 292440, 496800, 929160 and 1260762) have been carefully tested to obtain the most suitable mesh number and quality. The mesh number 929160 was used in this paper because it was found to provide high orthogonal quality of between 0.7 – 1, which can help obtain high-quality simulation results with suitable iteration time. For all the simulations reported here, the Courant-Friedrichs-Lewy number (CFL) is kept below 0.3, the dimensionless time step is 0.004, and the dimensionless wall distance of the first mesh near the walls is about 1.

3. Results and discussion

Three cases of rotational cylinder conditions have been addressed in this work. The first case (Case1) is when the cylinder is stationary ($\Omega = 0$). The second case (Case2) is when the rotational direction of the cylinder is clockwise ($\Omega < 0$), whereas the third case (Case3) is when the cylinder rotates in the anti-clockwise direction ($\Omega > 0$). For more information, when the cylinder rotates in the clockwise direction, it favours the lid-driven motion, unlike when the cylinder rotates in the anti-clockwise direction, which opposes the lid-driven wall movement.

3.1. Flow and thermal fields

Fig. 5 and Fig. 6, respectively, display the isotherms and streamlines contours, and iso-surface temperatures of pure water for Reynolds numbers Re = 5000 and 10000, and rotational

speeds, $-5 \leq \Omega \leq 5$ to show the influences of rotational speed and direction on the turbulent flow in the cavity. Essentially, it was demonstrated that the effect of increasing the Reynolds number is more significant when the cylinder is rotating in the anticlockwise direction. By focusing on the rotational speed condition, it can be seen that for both Reynolds numbers, and when the rotational move and lid-driven move were in the same direction, the forces of both movements supported each other, which led to rotating the whole fluid field in the same direction and producing a reduced number of secondary vortices, unlike when the lid-driven motion and rotational motion were in oppose directions, $1 \leq \Omega \leq 5$, which produces more secondary eddies within the domain, especially at higher values of Reynolds number and rotational speed. At $\Omega = 0$, it was demonstrated that the force of the top wall movement was driving the flow structure beyond the miner influence of the buoyancy effect. In the comparison between pure fluid and nanofluid, it can be clearly observed from Fig. 7 that involving a nanofluid has its positive influences on the flow patterns and heat distributions across all the study cases.

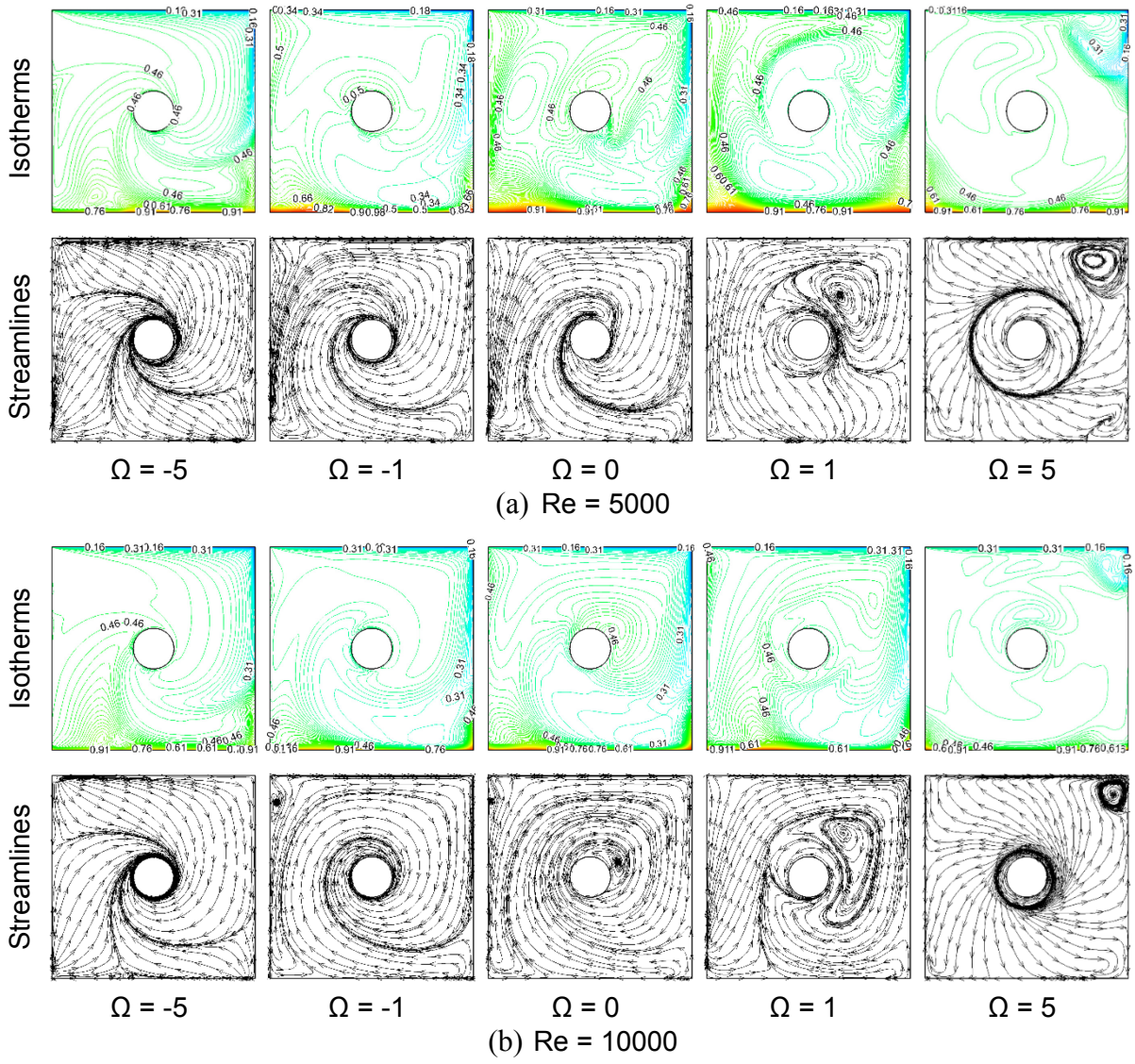

Fig. 5. Isotherms and streamlines contours for $\phi = 0$ at different Reynolds numbers and rotational speeds.

198

199

200

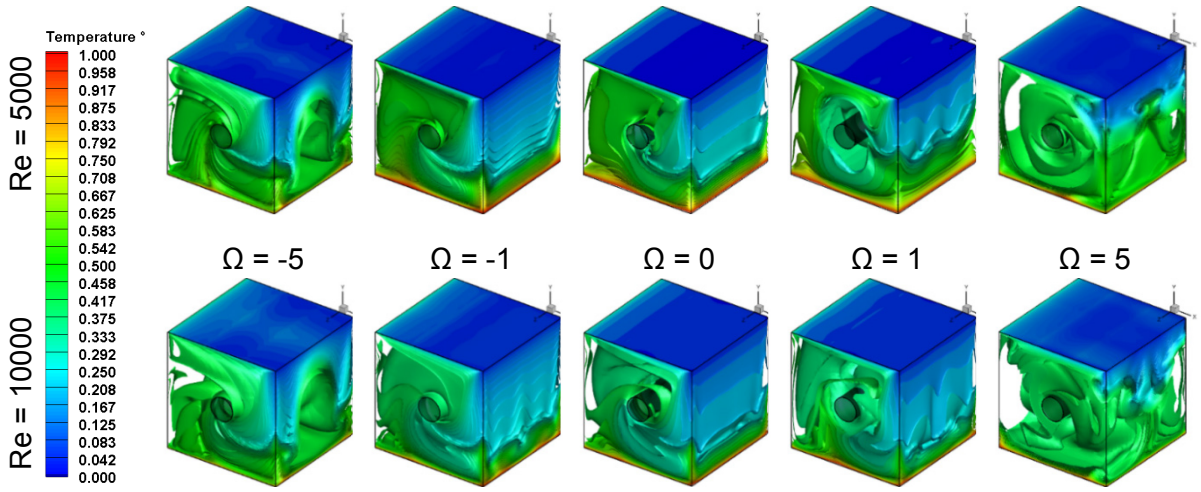

Fig. 6. Three-dimensional iso-surface profiles comparing the clockwise and anti-clockwise rotation of the cylinder for $\phi = 0$.

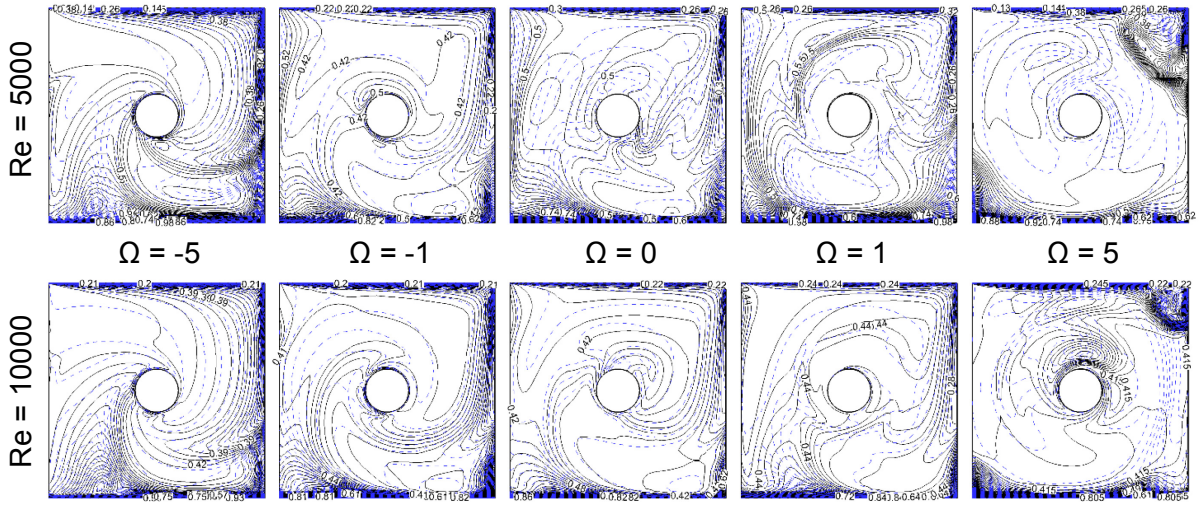

Fig. 7. Isotherm contour comparisons between pure fluid ($\phi = 0$, solid lines) and nanofluid ($\phi = 0.025$, broken lines) for different Reynolds numbers and rotational speeds.

3.2. Mean velocity profile

The variation of the mean velocity profiles of the horizontal lines at 0.25, 0, 0 and 0.25, 1, 0, for the pure water and nanofluid at Reynolds numbers of Re = 5000 - 10000 and rotational speeds $-5 \le \Omega \le 5$ are shown in Fig. 8. Generally, it can be observed that at all values of Reynolds number and rotational speed, the velocity near the moving wall is controlled by the lid movement. In addition, it might be noted that the effect of changing the rotating directions on the mean velocity profiles, especially at the bottom half of the geometry (*y*-axis height is 0.5 m), is less influenced by the moving top wall. Moreover, at $\Omega = 5$ and Re = 5000, it can be concluded that the rotating cylinder is controlling the velocity profile over the whole domain, unlike when the Reynolds number is increased to 10000, which limited the control of the

rotating cylinder to just the bottom part of the cavity. By effectively introducing nanoparticles into the pure water, it can be seen that for both Reynolds number values, the rotational speed of 5 had a significant influence on the whole flow domain.

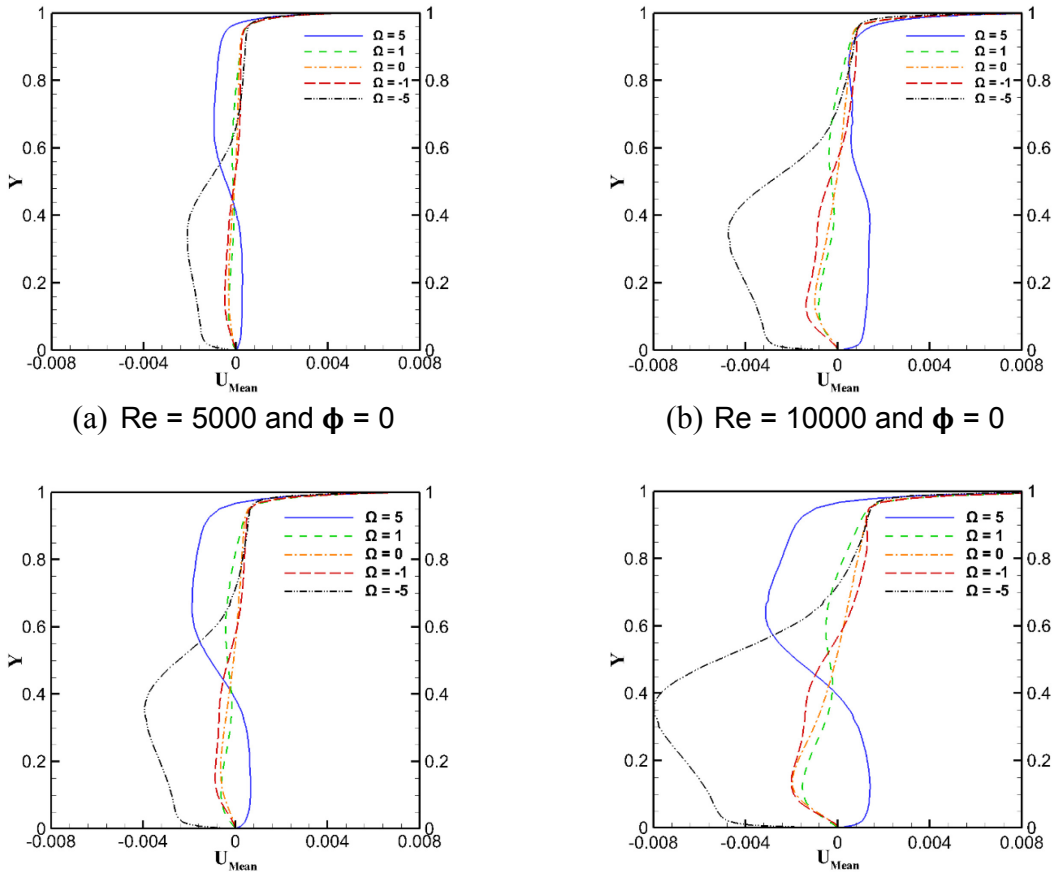

(a) Re = 5000 and ϕ = 0 (b) Re = 10000 and ϕ = 0

(c) Re = 5000 and ϕ = 0.025 (d) Re = 10000 and ϕ = 0.025

Fig. 8. Mean velocity profiles at vertical lines.

3.3. Wall shear stress

The wall shear stress can be calculated from the dynamic viscosity of the fluid multiplied by the fluid velocity gradient at the wall. The variations in the wall shear stress at the moving top wall and the heated bottom wall for the selected rotational cylinder speeds and directions for the two Reynolds number values are shown in Fig. 9. Clearly, at the top wall for both Reynolds numbers and a rotational speed within the range $-1 \leq \Omega \leq 5$, the wall shear stress values are essentially unchanged. This is due to the fact that, either a speed or direction change of the rotational cylinder could not affect the velocity profiles in the boundary layers near the top wall significantly, as shown in Fig. 8, though a noticeable effect was observed when the rotational speed became -5, suggesting that the boundary layer profile due to the top lid movement is now somewhat affected by the fluid motion due to the cylinder rotation. On the other hand, at the bottom wall, the wall shear stress is less affected by the moving top wall, and the rotational

cylinder plays a leading role in bottom wall shear stress. As a result, the wall shear distributions show certain variations for different rotation speeds and directions, reaching their maximum effect when the rotational speed reached -5. Clearly, the overall shear stress levels at the bottom wall are much lower in comparison to the top wall. Furthermore, the wall shear stresses are linked closely to the heat transfer coefficients, which will be discussed in more detail in section 3.5 below.

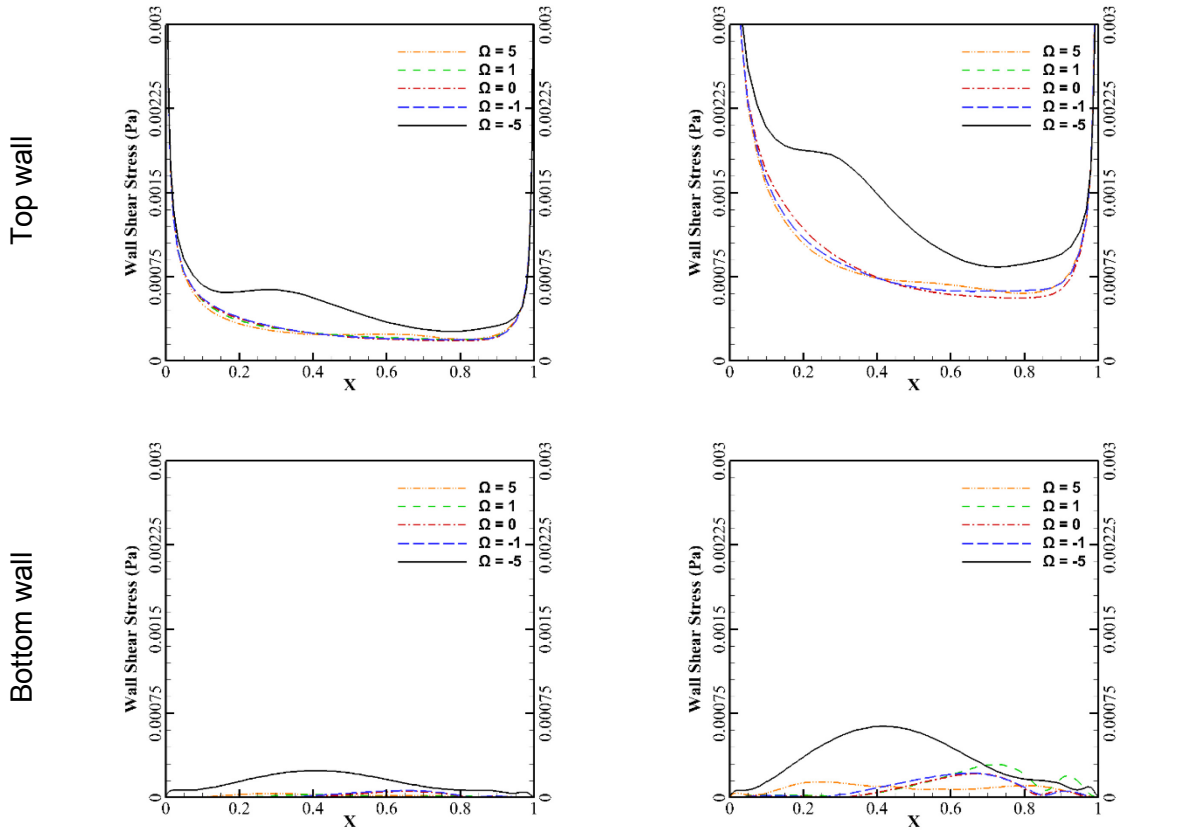

Fig. 9. Wall shear stress profiles for different rotational speeds and Reynolds numbers at the top and bottom walls.

3.4. Turbulent kinetic energy

It is well known that the root mean square (RMS) calculation of the fluid velocity fluctuations is defined as the turbulent kinetic energy (TKE), which represents the kinetic energy of the fluid motion per unit mass associated with the turbulent eddies. The averaged TKE profiles at the two selected positions, one at the mid-height between the centre of the cylinder and the bottom wall (y = 0.25) and the other at the mid-height between the cylinder centre and the top wall (y = 0.75) are shown in Fig. 10, which illustrates the effects of changing the cylinder at rotational speeds and directions for the two Reynolds number values of Re = 5000, and 10000. The simulated results indicate that for both Reynolds numbers, the TKE trend behaviours are more or less the same as for the corresponding rotational speed, though their magnitudes

increase significantly as the Reynolds number increases from 5000 (Fig. 10 a) to 10000 (Fig. 10 b). At either Reynolds number, it can be determined that the rotating cylinder has a substantial effect on the TKE profiles, especially with the rotational speed being -5 at y = 0.25 and with rotational speeds being of 5 and -5 at y, x = 0.75.

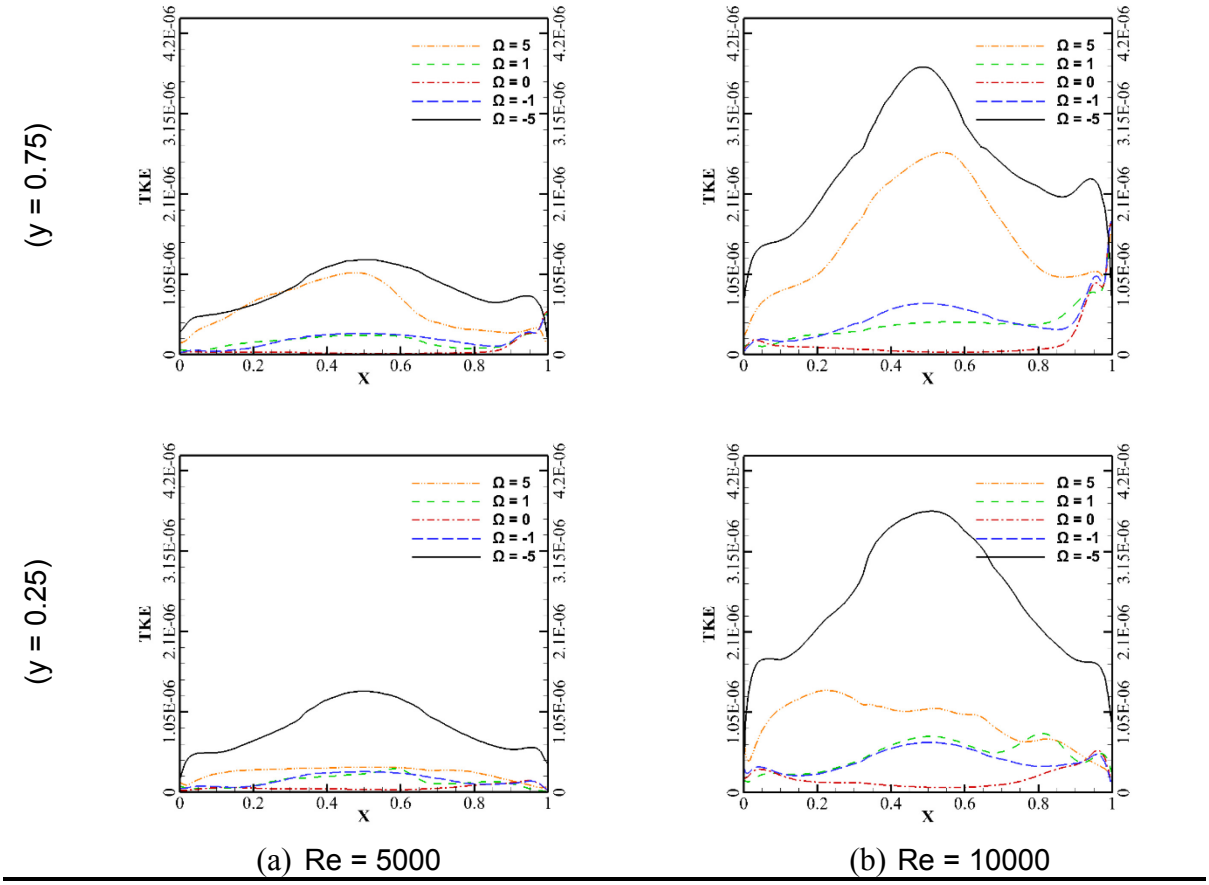

Fig. 10. Turbulence kinetic energy profiles for different rotational speeds and Reynolds numbers.

3.5. Nusselt number

It is widely recognised that heat transfer can be rapidly enhanced by involving turbulent flow, unlike when the flow is laminar. Which can develop an insulating blanket near the solid walls [28]. Any intermixing of the fluid would not happen when the flow motion is slow because the boundary layer velocity reduces smoothly due to the viscous drag, which can lead the heat transfer relying only on molecular convection and conduction. By contrast, the heat transfer rate can be enhanced significantly by incrementing the fluid velocity, which generates turbulent vortices where the boundary layers break away from the cavity walls and mix with the bulk of the fluid further from the obstructed enclosure walls [29]. Fig. 11 and Fig. 12 illustrate the local Nusselt number distributions for pure water and the nanofluid for the selected Reynolds numbers, Re = 5000 and 10000, and rotational speeds, $-5 \leq \Omega \leq 5$, for turbulent flow condition

at the midlines of the bottom and top walls, respectively. For both Reynolds numbers, the bottom wall Nusselt numbers are affected by changing either the rotational speed or the rotational direction. The combined motion of the moving top wall and rotating cylinder provide for higher local Nusselt numbers at the bottom wall, particularly when the rotational speed is -5. On the other hand, the influences of the rotational speed on the moving top wall for both Reynolds numbers are less remarkable unless the rotational speed is -5, as the heat transfer characteristics in this region are mainly controlled by the fluid motion due to the wall movement. It is worth noting that the heat transfer distributions at the top and bottom walls bear a close resemblance to the wall shear profiles, as discussed in section 3.3, which can be explained by the well-known Reynolds analogy between heat and momentum transfer. Both the top and bottom wall Nusselt numbers for pure water and the nanofluid at different Reynolds numbers and rotational speeds are compared in Table 2 to quantify the nanofluid's effect on the heat transfer coefficient. It can be observed that for all different Reynolds numbers and rotational speed cases, the effects of the nanofluid on the heat transfer coefficients were always positive, and were more visible at the bottom wall than at the top wall.

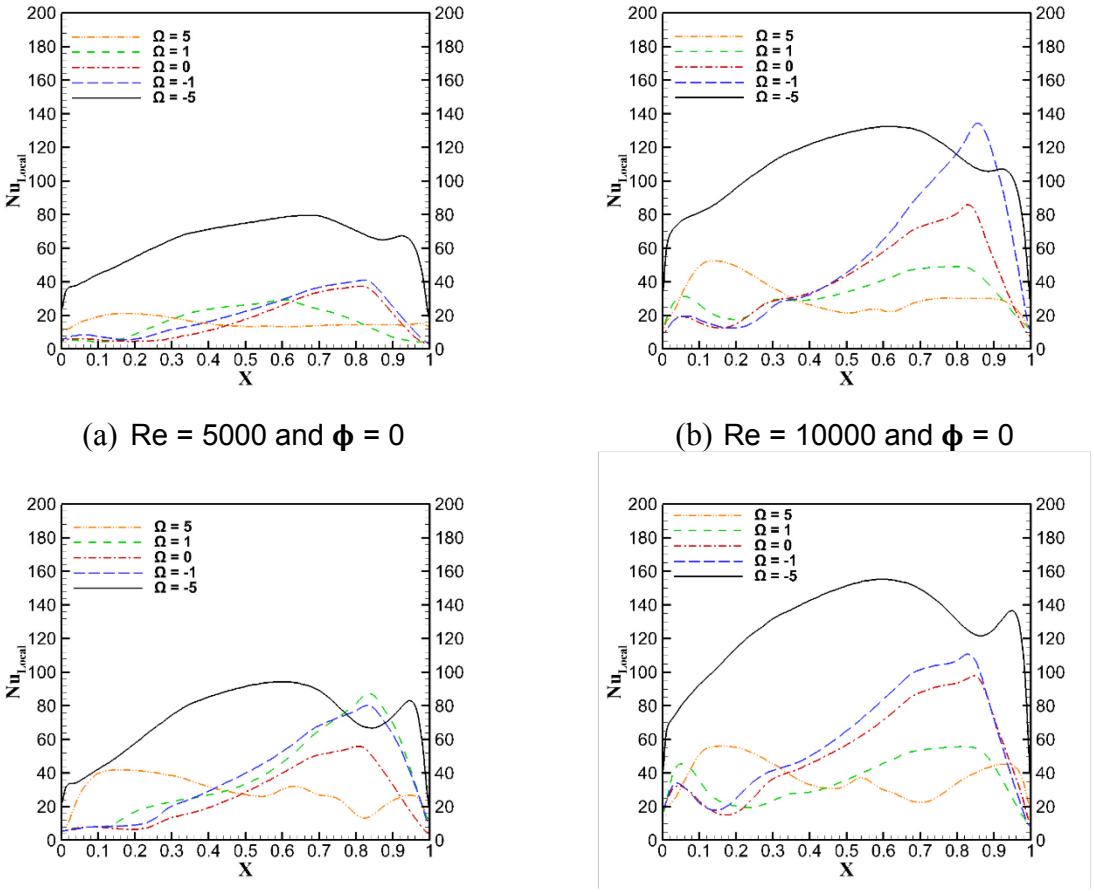

(a) Re = 5000 and ϕ = 0

(b) Re = 10000 and ϕ = 0

(c) Re = 5000 and ϕ = 0.025

(d) Re = 10000 and ϕ = 0.025

Fig. 11. Local Nusselt numbers at the bottom wall for pure fluid and nanofluid.

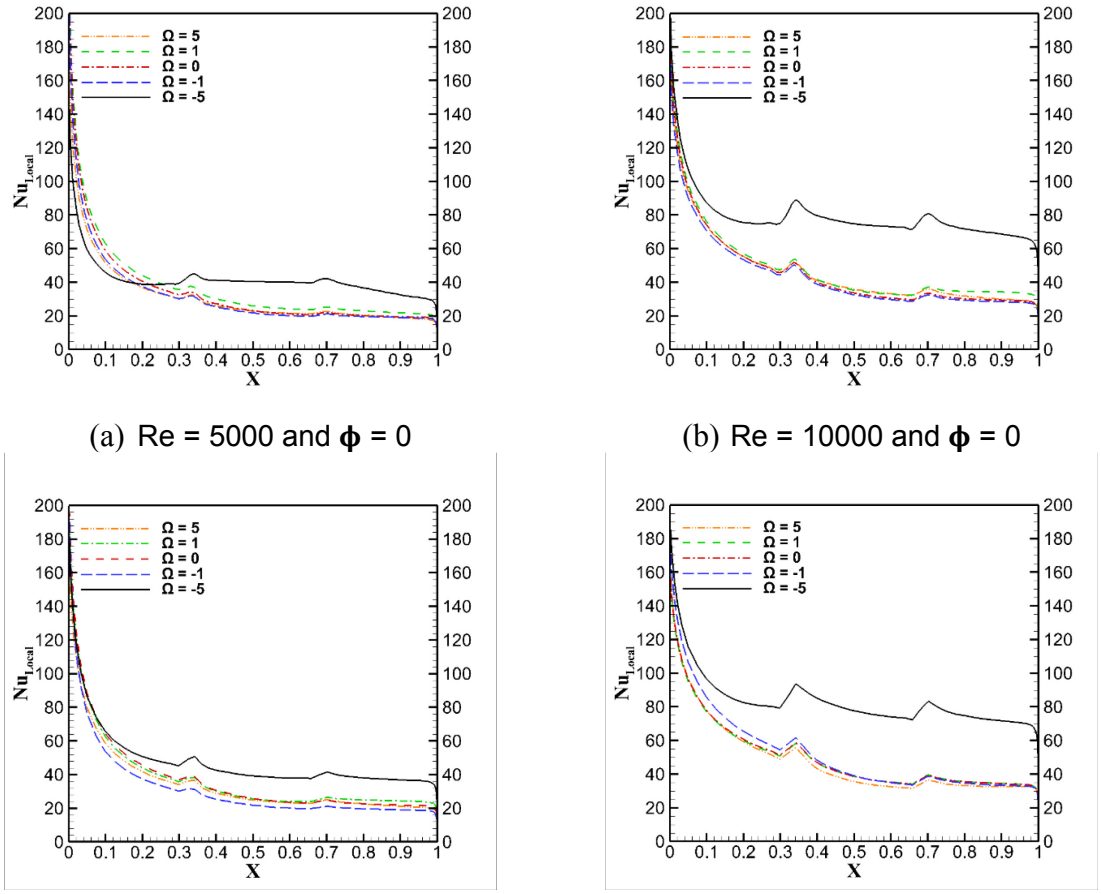

(a) Re = 5000 and ϕ = 0 (b) Re = 10000 and ϕ = 0

(c) Re = 5000 and ϕ = 0.025 (d) Re = 10000 and ϕ = 0.025

Fig. 12. Local Nusselt numbers at the top moving wall for pure fluid and nanofluid.

Table 2
Comparison of Average Nusselt numbers between pure fluid and nanofluid at the top and bottom walls.

Rotational speed		Ω = -5	Ω = -1	Ω = 0	Ω = 1	Ω = 5
Top	Nu_{nf}/Nu_{H2O} (Re = 5000)	59.97/55.41 = 1.08	50.24/41.76 = 1.20	47.11/44.77 = 1.05	46.99/47.85 = 0.98	42.78/39.74 = 1.07
	Nu_{nf}/Nu_{H2O} (Re = 10000)	87.85/84.20 = 1.04	58.63/50.39 = 1.16	55.65/53.17 = 1.04	55.29/55.89 = 0.98	54.00/53.24 = 1.01
Bottom	Nu_{nf}/Nu_{H2O} (Re = 5000)	63.92/56.83 = 1.12	31.83/17.14 = 1.85	21.74/14.26 = 1.52	31.92/14.40 = 2.21	25.14/14.85 = 1.69
	Nu_{nf}/Nu_{H2O} (Re = 10000)	113.48/96.0 0 = 1.18	32.23/28.96 = 1.11	50.31/34.98 = 1.43	45.76/44.82 = 2.02	33.44/26.80 = 1.24

4. Conclusion

In this paper, the mixed turbulent convection heat transfer of a 3D lid-driven cavity containing a cylinder that could rotate either clockwise or anticlockwise is addressed by involving both pure water and the nanofluid. The simulations cover a range of cylinder rotation speeds, -5 ≤

Ω ≤ 5, and Reynolds numbers, Re = 5000 and 10000, through the URANS method. The following points have been concluded from this research:

- The temperature distributions and flow patterns were found to be influenced by both the speed values and the direction in which the cylinder was rotating, and nanofluid always positively effectives the heat transfer enhancement.
- The bottom wall shear stress can be influenced by both the rotational speeds and the Reynolds numbers, whereas the top wall shear stress values remain roughly the same for different rotational speeds and directions, except when Ω = -5.
- When Ω = -5, the lowest number of secondary eddies was found and the highest Nusselt number observed, especially in the case of the latter when the nanofluid was involved, unlike when Ω = 5 where the highest number of secondary vortices was produced.
- The cylinder rotation speed has a weaker influence on the top wall than on the bottom wall, where the largest difference in bottom wall Nusselt number between the conventional fluid and the nanofluid was found at a rotational speed of Ω = 1.

Acknowledgements

The authors would like to thank the Ministry of Higher Education of Scientific Research of Iraq for supporting this project financially.

References

[1] A.K. Kareem, S. Gao, A.Q. Ahmed, Unsteady simulations of mixed convection heat transfer in a 3D closed lid-driven cavity, International Journal of Heat and Mass Transfer, 100 (2016) 121-130.

[2] D. Chatterjee, B. Mondal, P. Halder, Hydromagnetic mixed convective transport in a vertical lid-driven cavity including a heat conducting rotating circular cylinder, Numerical Heat Transfer, Part A: Applications, 65(1) (2014) 48-65.

[3] S. Hussain, S. Ahmad, K. Mehmood, M. Sagheer, Effects of inclination angle on mixed convective nanofluid flow in a double lid-driven cavity with discrete heat sources, International Journal of Heat and Mass Transfer, 106 (2017) 847-860.

[4] C.-C. Liao, C.-A. Lin, Mixed convection of a heated rotating cylinder in a square enclosure, International Journal of Heat and Mass Transfer, 72 (2014) 9-22.

[5] R. Roslan, H. Saleh, I. Hashim, A. Bataineh, Natural convection in an enclosure containing a sinusoidally heated cylindrical source, International Journal of Heat and Mass Transfer, 70 (2014) 119-127.

[6] A. Ben-Nakhi, A.J. Chamkha, Conjugate natural convection around a finned pipe in a square enclosure with internal heat generation, International Journal of Heat and Mass Transfer, 50(11) (2007) 2260-2271.

[7] A.K. Kareem, S. Gao, Mixed convection heat transfer of turbulent flow in a three-dimensional lid-driven cavity with a rotating cylinder, International Journal of Heat and Mass Transfer, 112(Supplement C) (2017) 185-200.

[8] A. Khaleel, S. Gao, CFD Investigation of Turbulent Mixed Convection Heat Transfer in a Closed Lid-Driven Cavity, World Academy of Science, Engineering and Technology, International Journal of Civil, Environmental, Structural, Construction and Architectural Engineering, 9(12) (2015) 1564-1569.

[9] C. Sun, B. Yu, H.F. Oztop, Y. Wang, J. Wei, Control of mixed convection in lid-driven enclosures using conductive triangular fins, International Journal of Heat and Mass Transfer, 54(4) (2011) 894-909.

[10] H.F. Oztop, Z. Zhao, B. Yu, Fluid flow due to combined convection in lid-driven enclosure having a circular body, International Journal of Heat and Fluid Flow, 30(5) (2009) 886-901.

[11] K.M. Gangawane, Computational analysis of mixed convection heat transfer characteristics in lid-driven cavity containing triangular block with constant heat flux: Effect of Prandtl and Grashof numbers, International Journal of Heat and Mass Transfer, 105 (2017) 34-57.

[12] K. Mehmood, S. Hussain, M. Sagheer, Mixed convection in alumina-water nanofluid filled lid-driven square cavity with an isothermally heated square blockage inside with magnetic field effect: Introduction, International Journal of Heat and Mass Transfer, 109 (2017) 397-409.

[13] S. Mirzakhanlari, K.M. Shirvan, M. Mamourian, A.J. Chamkha, Increment of mixed convection heat transfer and decrement of drag coefficient in a lid-driven nanofluid-filled cavity with a conductive rotating circular cylinder at different horizontal locations: A sensitivity analysis, Powder Technology, 305 (2017) 495-508.

[14] R. Shyam, M. Sairamu, N. Nirmalkar, R. Chhabra, Free convection from a heated circular cylinder in confined power-law fluids, International Journal of Thermal Sciences, 74 (2013) 156-173.

[15] S.A. Nabavizadeh, S. Talebi, M. Sefid, M. Nourmohammadzadeh, Natural convection in a square cavity containing a sinusoidal cylinder, International journal of thermal sciences, 51 (2012) 112-120.

[16] B. Souayeh, N. Ben-Cheikh, B. Ben-Beya, Numerical simulation of three-dimensional natural convection in a cubic enclosure induced by an isothermally-heated circular cylinder at different inclinations, International Journal of Thermal Sciences, 110 (2016) 325-339.

[17] A.K. Kareem, S. Gao, Computational study of unsteady mixed convection heat transfer of nanofluids in a 3D closed lid-driven cavity, International Communications in Heat and Mass Transfer, 82 (2017) 125-138.

[18] F. Garoosi, F. Hoseininejad, Numerical study of natural and mixed convection heat transfer between differentially heated cylinders in an adiabatic enclosure filled with nanofluid, Journal of Molecular Liquids, 215 (2016) 1-17.
[19] A.K. Kareem, H. Mohammed, A.K. Hussein, S. Gao, Numerical investigation of mixed convection heat transfer of nanofluids in a lid-driven trapezoidal cavity, International Communications in Heat and Mass Transfer, 77 (2016) 195-205.
[20] F.M. White, Fluid mechanics, WCB, ed: McGraw-Hill, Boston, (1999).
[21] H.K. Versteeg, W. Malalasekera, An introduction to computational fluid dynamics: the finite volume method, Pearson Education, 2007.
[22] P. Huang, J. Bardina, T. Coakley, Turbulence Modeling Validation, Testing, and Development, NASA Technical Memorandum, 110446 (1997).
[23] B. Ghasemi, S. Aminossadati, Brownian motion of nanoparticles in a triangular enclosure with natural convection, International Journal of Thermal Sciences, 49(6) (2010) 931-940.
[24] A. Mohamad, R. Viskanta, Flow and heat transfer in a lid-driven cavity filled with a stably stratified fluid, Applied mathematical modelling, 19(8) (1995) 465-472.
[25] A. FLUENT, 15.0 Theory Guide, Ansys Inc, 5 (2013).
[26] D. Chatterjee, S.K. Gupta, B. Mondal, Mixed convective transport in a lid-driven cavity containing a nanofluid and a rotating circular cylinder at the center, International Communications in Heat and Mass Transfer, 56 (2014) 71-78.
[27] M. Alinia, D. Ganji, M. Gorji-Bandpy, Numerical study of mixed convection in an inclined two sided lid driven cavity filled with nanofluid using two-phase mixture model, International Communications in Heat and Mass Transfer, 38(10) (2011) 1428-1435.
[28] 525 East Stop 18 Road Greenwood, IN 46142 317-887-0729 fax: 317-881-1277, cotns 8/2/01, REVISION 10/25/95, original created 9/6/95 © 2001 ADVANTAGE ENGINEERING, INC, in, www.advantageengineering.com.
[29] HRS Heat Exchangers Ltd, 10-12 Caxton Way, Watford Business Park, Hertfordshire WD18 8JY, UK, in, https://www.hrs-heatexchangers.com/resource/comparison-laminar-turbulent-flow/.